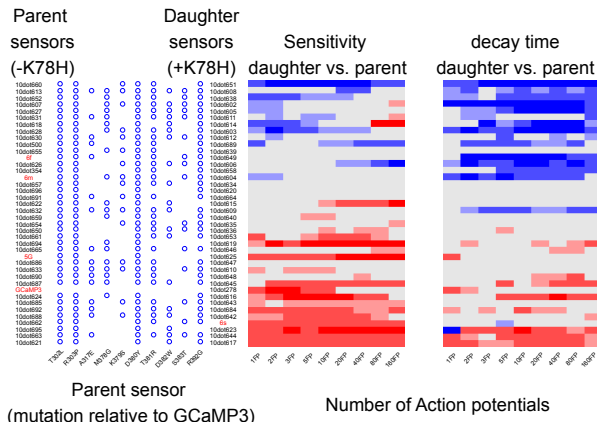


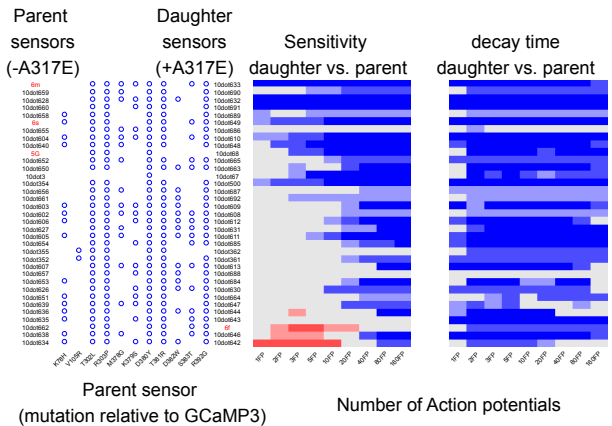
Supplementary Figure 1 | Neuronal culture screening results.

Results from the neuronal culture screen. The inverse of the fluorescence half decay time (stimulus, 10 action potentials) is plotted versus peak $\Delta F/F_0$ (stimulus, 1 action potential) for GCaMP3, 5G, 6s, 6m, 6f, OGB1 and 442 other GCaMP variants. The symbol color represents the inverse p-value for $\Delta F/F_0$ (1 action potential) (relative to GCaMP3). The symbol area is proportional to the normalized basal fluorescence (F_0) (relative to GCaMP3).

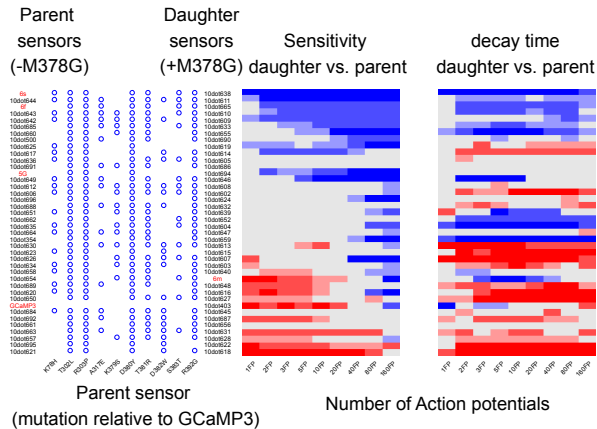
Effect of K78H



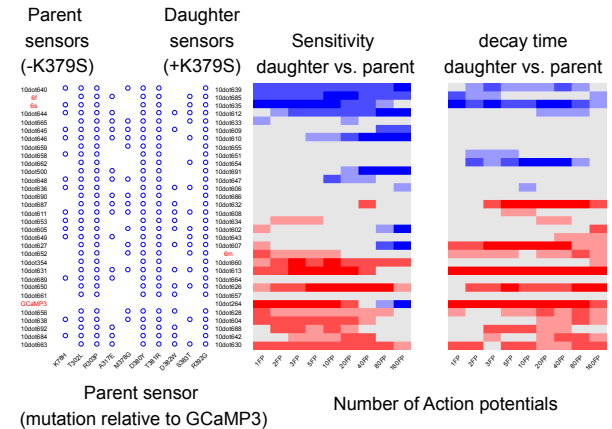
Effect of A317E



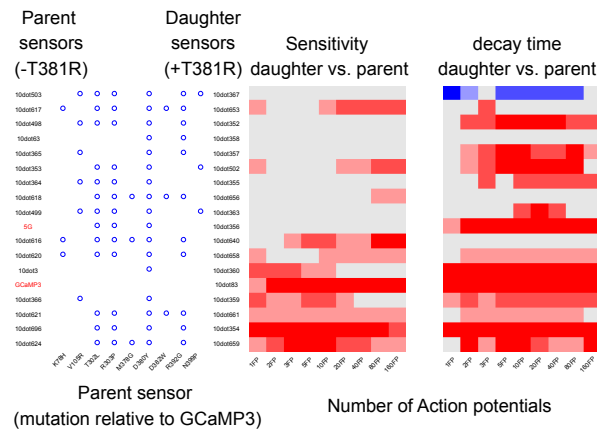
Effect of M378G



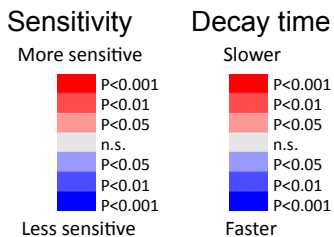
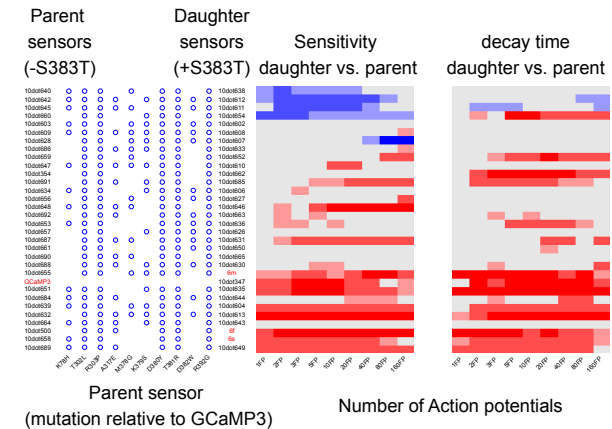
Effect of K379S



Effect of T381R

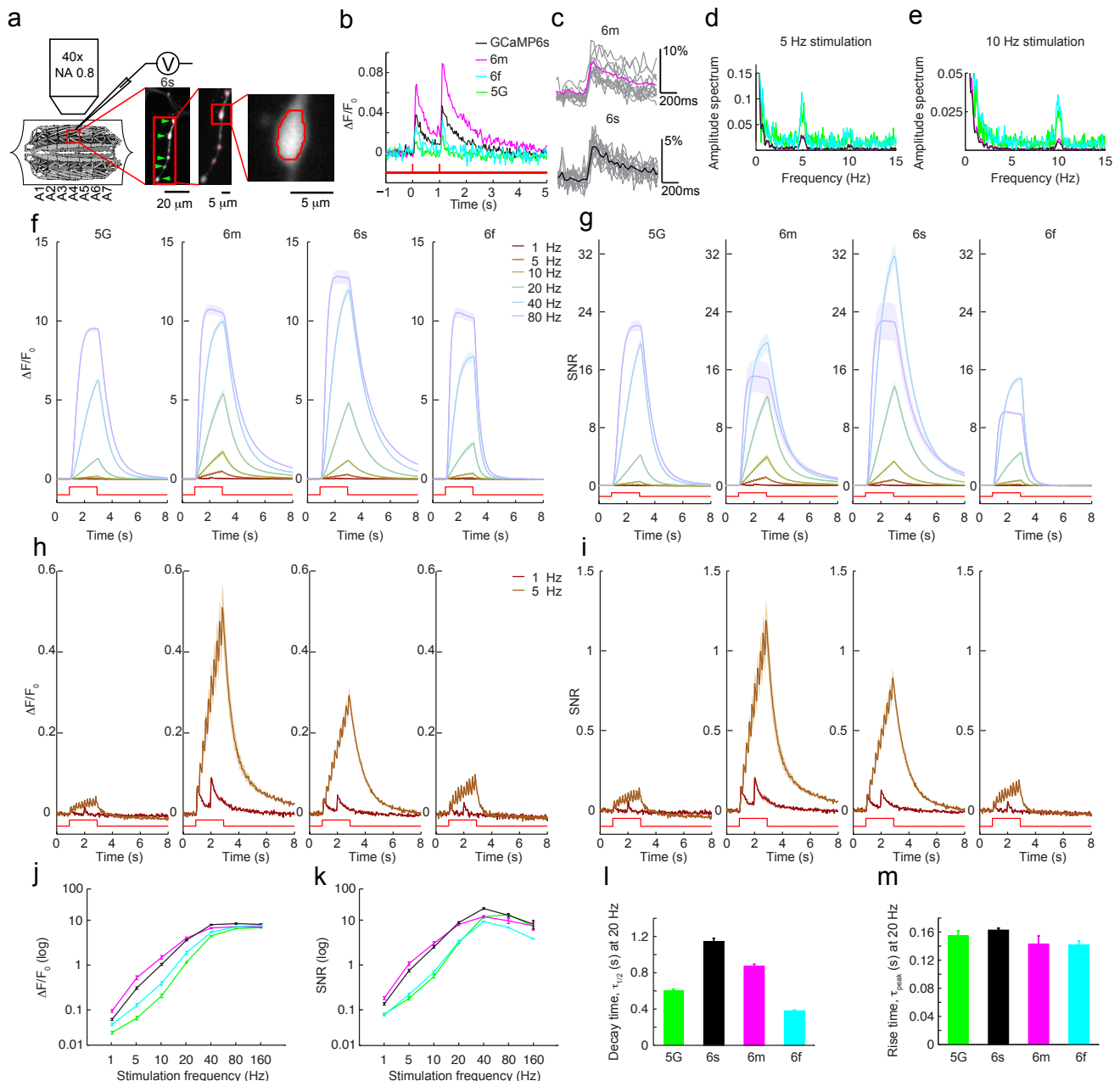


Effect of S383T



Supplementary Figure 2 | Effects of point mutations on different GCaMP variants.

Each panel illustrates a single point mutation. The left column of each panel shows the identity of the parent sensor (mutations relative to GCaMP3) on which the point mutation was made. The middle column of each panel shows the change in sensitivity (color coded; red, more sensitive; blue, less sensitive; gray, not significant) after adding the point mutation to the parent sensors indicated on the left. The right column shows the change in decay time (color coded; red, slower; blue, faster; gray, not significant) after adding the point mutation to the parent sensors indicated on the left.


Supplementary Figure 3 | Imaging activity in *Drosophila* larval NMJ boutons with GCaMP5 and GCaMP6 variants.

a, Schematic of larval NMJ stimulation and imaging, epifluorescence (green arrow heads), and high magnification $\Delta F/F_0$ images of Type 1b boutons from muscle 13 (segments A3-A5). Experiments were performed as previously described¹⁶.

b, Averaged fluorescence transients after 1 Hz stimulus for 2 s for GCaMP5G, 6f, 6m, and 6s (green, cyan, magenta, black; $n=10, 12, 14, 12$ FOVs, respectively).

c, Single trial fluorescence transients (gray) produced by single action potentials. Median traces for GCaMP6m (magenta) and 6s (black).

d, Fourier spectra normalized to 0 Hz of fluorescence signal acquired during 5 Hz stimulation.

e, Same as **d** for 10 Hz stimulus.

f, Average $\Delta F/F_0$ (\pm s.e.m) traces recorded after 1, 5, 10, 20, 40, and 80 Hz stimulus for 2 s (red).

g, Average SNR traces.

h, Average $\Delta F/F_0$ traces recorded after 1 and 5 Hz stimulus for 2 s.

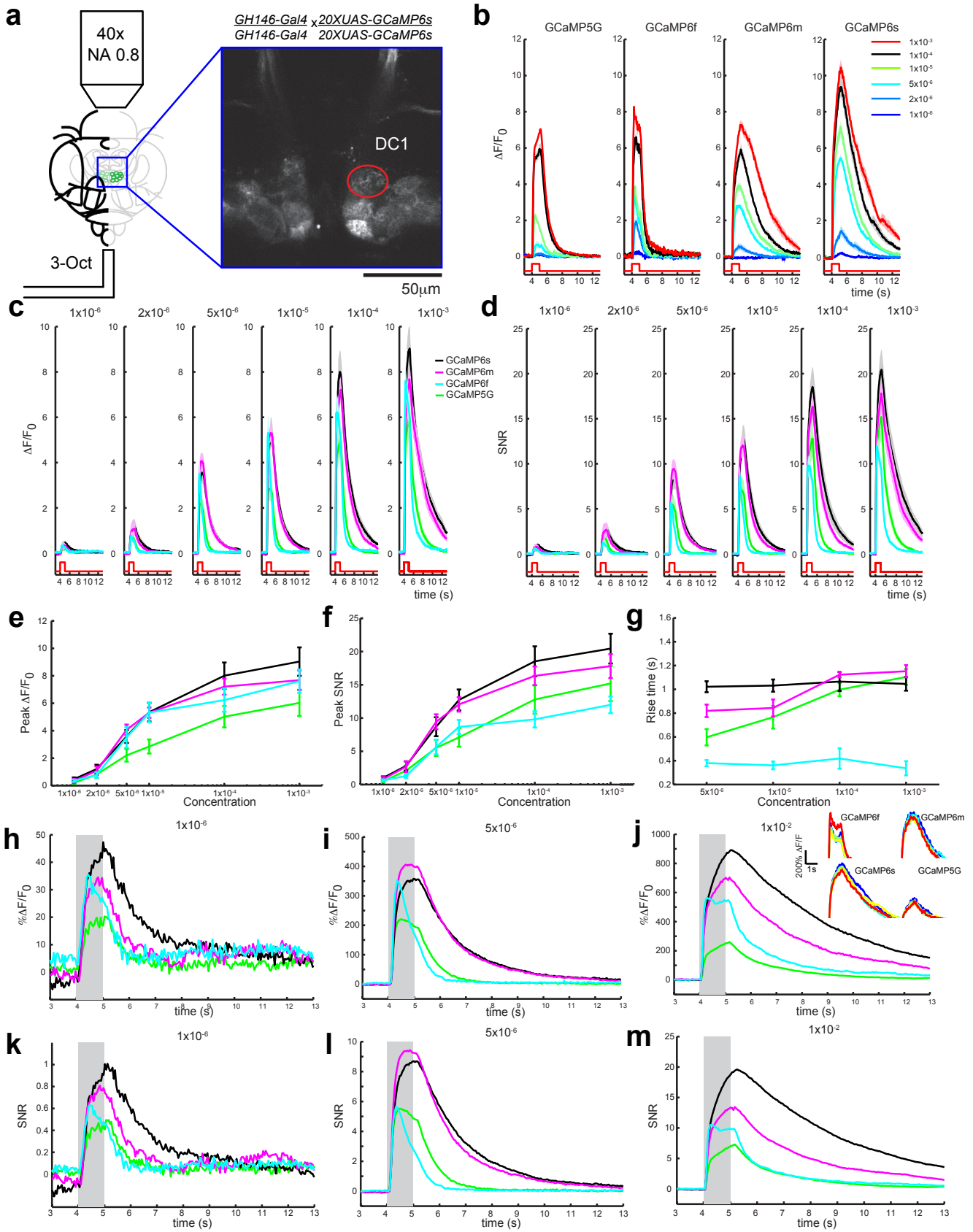
i, Average SNR traces for 1 and 5 Hz stimulus for 2 s.

j, Average peak $\Delta F/F_0$ from 1-160 Hz.

k, Average peak SNR from 1-160 Hz.

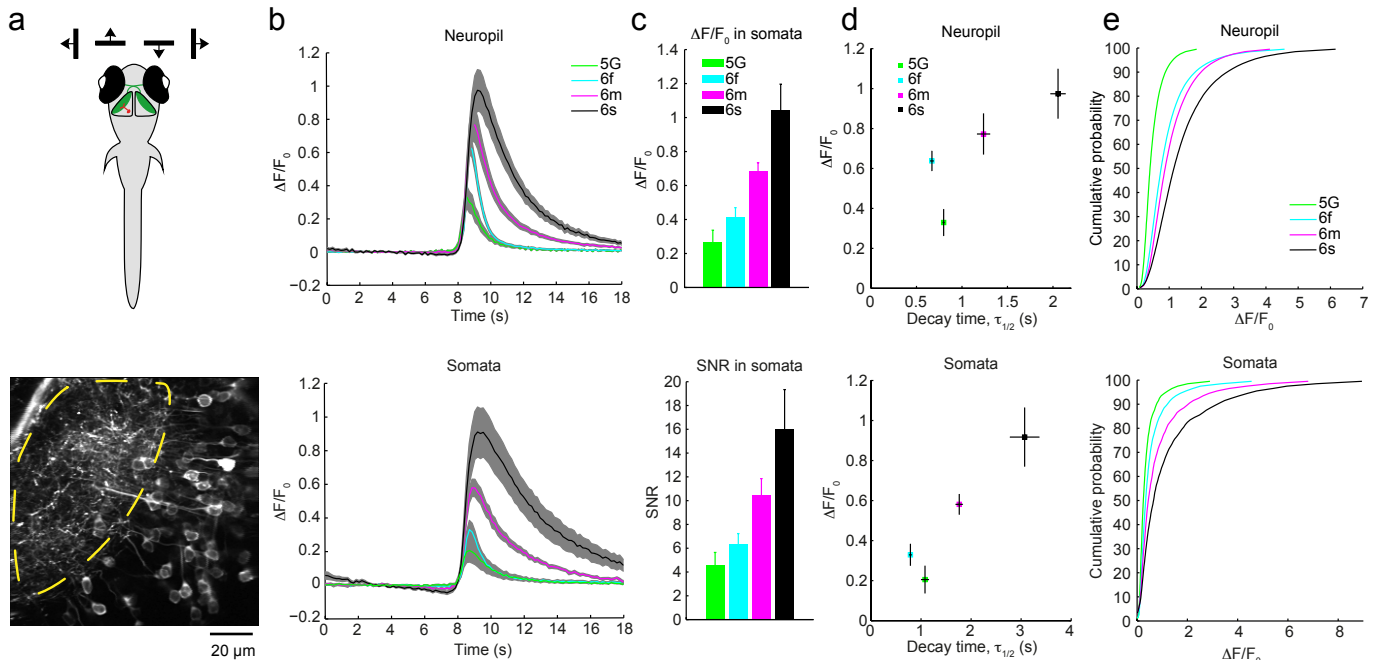
l, Average half decay time after 20 Hz stimulation for 2 s.

m, Average rise time to peak after stimulus offset after 20 Hz stimulation for 2 s.



Supplementary Figure 4 | Imaging activity in the antennal lobe of GCaMP5G and GCaMP6 variants of *Drosophila* in an olfactory assay.

- a**, Schematic of awake head-restrained fly presented with odor and imaged on two-photon microscope as described previously¹⁶. Laser: mode-locked Ti:Sapphire, 925 nm, back aperture power: ~7 mW. Odor: 3-octanol, diluted in paraffin oil (both from Sigma) and again in air via custom olfactometer. We imaged the DC1 glomerulus (red oval, *GH146-Gal4/GH146-Gal4 x UAS-GCaMP6s/UAS-GCaMP6s* fly) at 20 Hz. All flies were females, 3 days after eclosion, raised in 16:8 light/dark cycle at 25°C, and imaged within 2 h after Light-On.
- b**, Sample results showing responses of antennal lobe DC1 projection neurons expressing GCaMP5G and GCaMP6 variants to 3-octanol at concentrations from 0.0001% to 0.1%. Odor pulse indicated by red lines at bottom. Fluorescence transients ($\Delta F/F_0$) color-coded by concentration. Each curve is the average of 5 consecutive repeats with thickness indicating standard error of mean (s.e.m.).
- c**, Comparison of sensitivity of GCaMP5G and GCaMP6 variants in the olfactory assay, with GCaMP variants color-coded. Each curve is the mean response \pm s.e.m. (GCaMP6s in black: 12 antennal lobes (ALs) in 8 flies; GCaMP6m in magenta: 12 ALs in 6 flies; GCaMP6f in cyan: 12 ALs in 6 flies; GCaMP5G in green: 10 ALs in 5 flies).
- d**, Comparison of the signal-to-noise ratio of GCaMP5G and GCaMP6 variants in olfactory assay, with the same data set as in panel **c**. Each curve represents the mean response \pm s.e.m.
- e**, Concentration tuning curves of peak $\Delta F/F_0$ of GCaMP5G and GCaMP6 variants. Error bars represent s.e.m.
- f**, Concentration tuning curves of peak SNR of GCaMP5G and GCaMP6 variants. Error bars represent s.e.m.
- g**, Comparison of times from onset of odor delivery to peak response of GCaMP5G and GCaMP6 variants during the odor assay. GCaMP6f is faster to peak than the others.
- h-j**, Comparison of mean $\Delta F/F_0$ of GCaMP5G and GCaMP6 variants during odor delivery at concentrations of 0.0001%, 0.0005% and 1% respectively. The gray shaded background shows odor delivery times. For **j**, GCaMP6s: 13 ALs in 10 flies; GCaMP6m: 15 ALs in 8 flies; GCaMP6f: 12 ALs in 7 flies; GCaMP5G: 9 ALs in 7 flies. Inset in **j** shows peak dynamics (starting from $\Delta F/F_0 = 300\%$) of single trial $\Delta F/F_0$ for GCaMP5G and GCaMP6 variants during one experiment. Each trace represents fluorescence signal from single trial in single field of view, and different repeats are color-coded. Onset and offset responses are clearly visible in GCaMP6f at the highest concentration of 1%.
- k-m**, Comparison of mean SNR of GCaMP5G and GCaMP6 variants at concentrations of 0.0001%, 0.0005% and 1% respectively, corresponding to **h-j**.



Supplementary Figure 5 | Imaging activity in the zebrafish optic tectum with GCaMP5G and GCaMP6 variants.

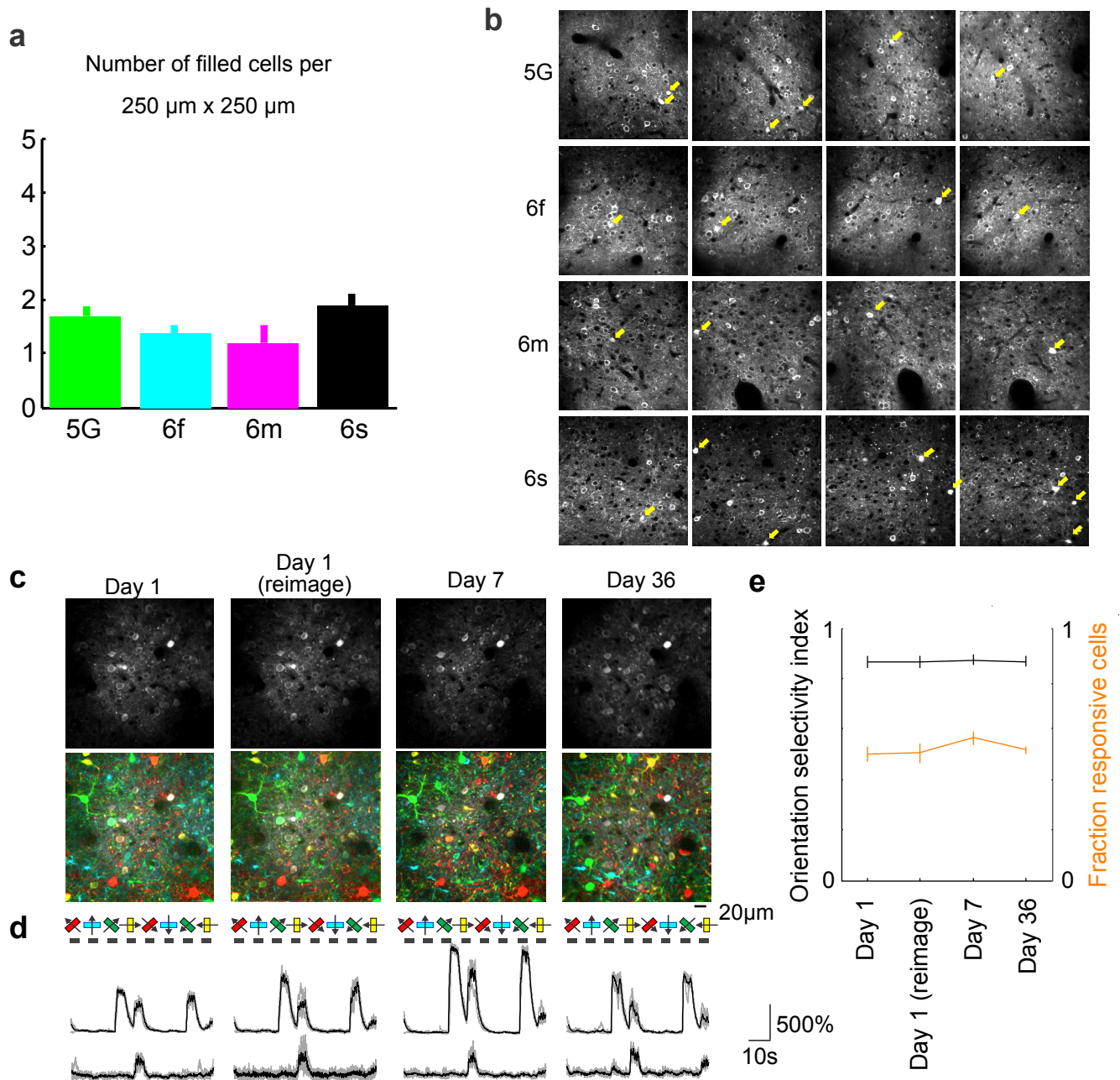
a, Top, schematic representation of tectal areas imaged in larval zebrafish. Neuropil and tectal somata responses were recorded during stimulation with an oriented bar, moving in one of four different directions. Bottom, z-projection of an image stack from an HuC:Gal4FF/UAS:GCaMP6s expressing larva showing mosaic expression in the neuropil (dashed yellow line) and tectal somata. *Nacre* (*mitfa*^{-/-}) or *casper* (*mitfa*^{-/-}, *roy*^{-/-}) zebrafish^{65,66} were maintained under standard conditions at 28°C and a 14:10 hour light:dark cycle⁶⁷ and larvae were raised in E3 embryo medium (5 mM NaCl, 0.17 mM KCl, 0.33 mM CaCl₂ and 0.33 mM MgSO₄). To obtain mosaic expression of GCaMP variants, embryos were injected at the 1-2 cell stage with 12 ng/μL plasmid DNA encoding Gal4FF⁶⁸ under the control of the pan-neuronal *elavl3*/HuC promoter (*elavl3*:Gal4FF), 8 ng/μL plasmid DNA encoding GCaMP5G or a GCaMP6 variant downstream of four non-repeating upstream activation sequences⁶⁹, and 40 ng/μL Tol2 transposase mRNA diluted in E3 medium with 0.025% phenol red. Inverted Tol2 repeats flanking the expression cassettes allowed for efficient genomic integration.

b, Calcium transients in tectal neuropil (top) and somata (bottom) of GCaMP5G (n=11 fish) and GCaMP6s, 6m, and 6f (n=11, 9, and 11, respectively) expressing fish. The traces show $\Delta F/F_0$ (mean \pm s.e.m.) averaged over all stimulus directions. Larvae were mounted as in previous studies¹⁷ and imaged at 6 d post-fertilization (dpf) using a custom-built two-photon microscope with a mode-locked Ti:Sapphire laser system (Spectra-Physics) tuned to 920 nm and a water immersion objective (XLUM Plan FLN 20X/1.0 W; Olympus). Images of the neuropil as well as somata of stratum periventriculare neurons were acquired at 5.85 Hz using software custom-written in LabView (National Instruments). Visual stimuli were presented on a flat opal glass screen underneath the larvae using a Microvision PicoP laser projector and a long pass filter (590 nm). A black bar of 1 mm thickness sweeping at 2 cm/s across a red 4.2 x 4.2 cm square centered on the fish was alternated in four cardinal directions. Each direction was presented three times. Each imaging plane consists of a neuropil region, containing processes from many neurons, and a region of mosaically labeled somata. Soma ROIs were selected manually by mouse-clicking on the centers, and the boundaries of the neuropil regions were also chosen by hand. Fluorescence traces were then automatically extracted, averaged over 3.15 μm radius circular regions of interest for the somata and 6.3 μm squares tiling the neuropil region with 3.15 μm steps, using Matlab (Mathworks) scripts. Baseline fluorescence (F_0) was defined as the median fluorescence in a 2 s period prior to the stimulus onset, minus the light level detected with the laser attenuated by a Pockels cell, and each response trace was converted to units of $\Delta F/F_0$. Because different cells will respond with varying latencies, in order to generate average response traces for comparison of kinetics, each individual trace was first aligned in time to be maximally correlated with the average. SNR was calculated by dividing the fluorescence change by the standard deviation of the point-to-point difference during the baseline period. Peak $\Delta F/F$ and SNR were the maximum single frame values recorded during stimulus presentation. Decay time was defined as the time taken for the average trace to fall to half its maximum value from the peak. All data points and error bars shown are the mean and s.e.m. values across different fish

c, Average peak $\Delta F/F_0$ and peak SNR values (\pm s.e.m.) of somata responses.

d, Half decay time of neuropil or somata responses plotted versus peak of average $\Delta F/F_0$ values (\pm s.e.m.).

e, The distribution of fluorescence responses across neuropil regions and somata.



Supplementary Figure 6 | Long-term expression of different GCaMP variants in the mouse visual cortex.

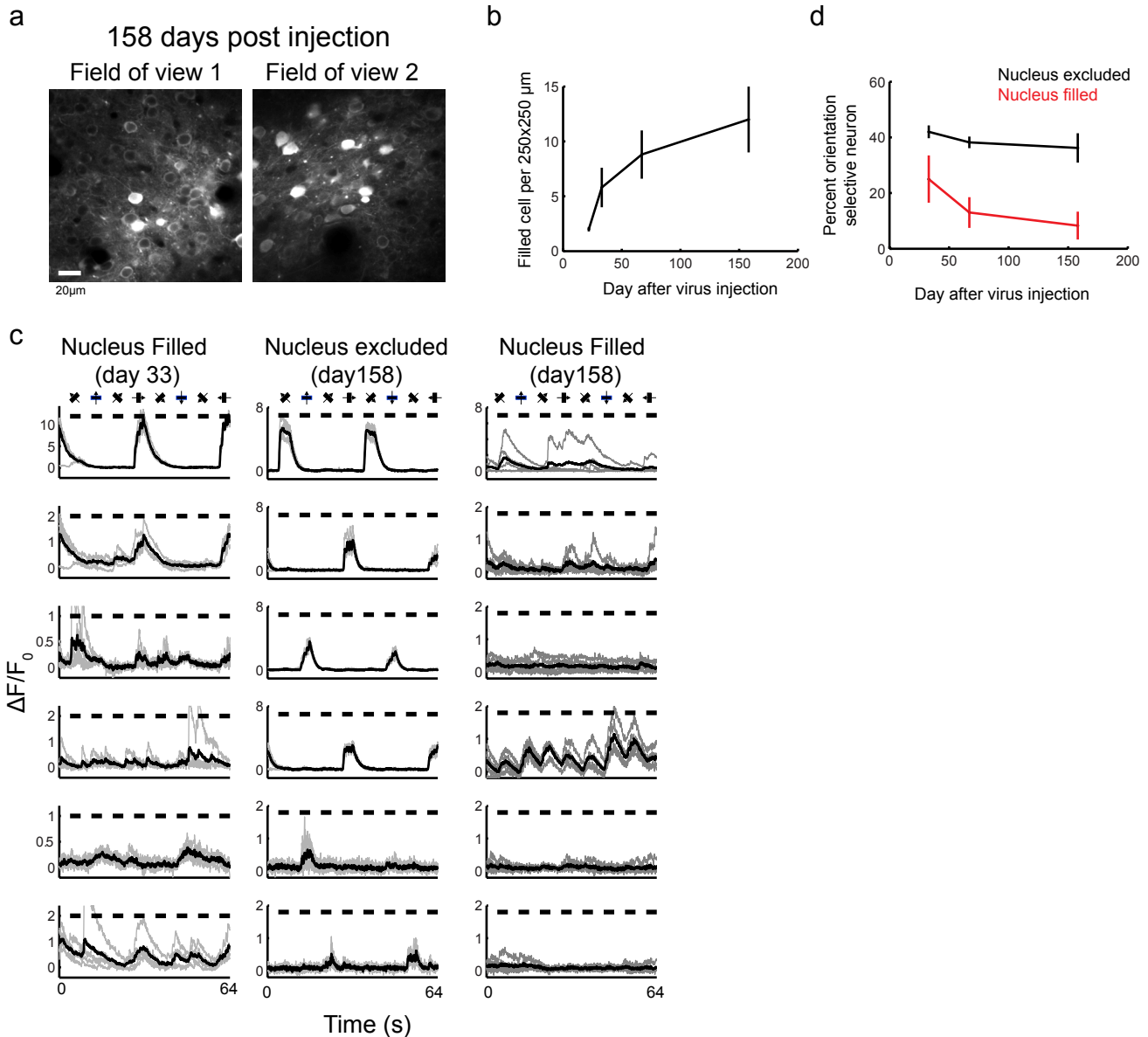
a, Average number of cells showing nuclear GCaMP fluorescence (filled cell) per 250 x 250 μm FOV (n=39, 38, 8, 20 fields of view for GCaMP5G, 6f, 6m and 6s, respectively).

b, Example fields of view for GCaMP5G, 6f, 6m, and 6s (4 fields shown per GCaMP variant) after 21-28 d of expression. Arrows indicate cells showing nuclear GCaMP fluorescence.

c, Representative field of view (GCaMP6s) imaged over one month. Top, raw fluorescence. Bottom, orientation selectivity map overlaid on raw fluorescence.

d, Orientation-selective responses for two example neurons imaged in multiple sessions.

e, The mean orientation selectivity index (left axis) and fraction of responsive neurons (right axis)



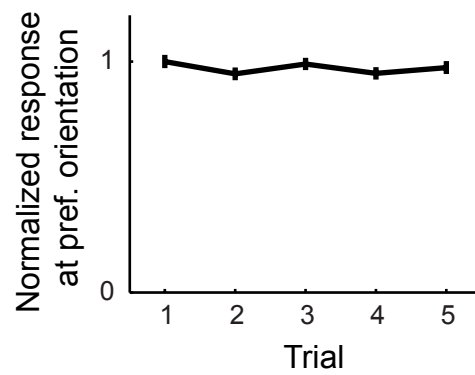
Supplementary Figure 7 | Long term expression of GCaMP6s in the mouse visual cortex.

a, Example images of V1 neurons 158 days after infection with AAV-*syn*-GCaMP6s-WPRE. Some fields of view had relatively few cells with filled nuclei (left); whereas others had more filled neurons (right).

b, Average number of cells showing nuclear GCaMP fluorescence as a function of time post infection.

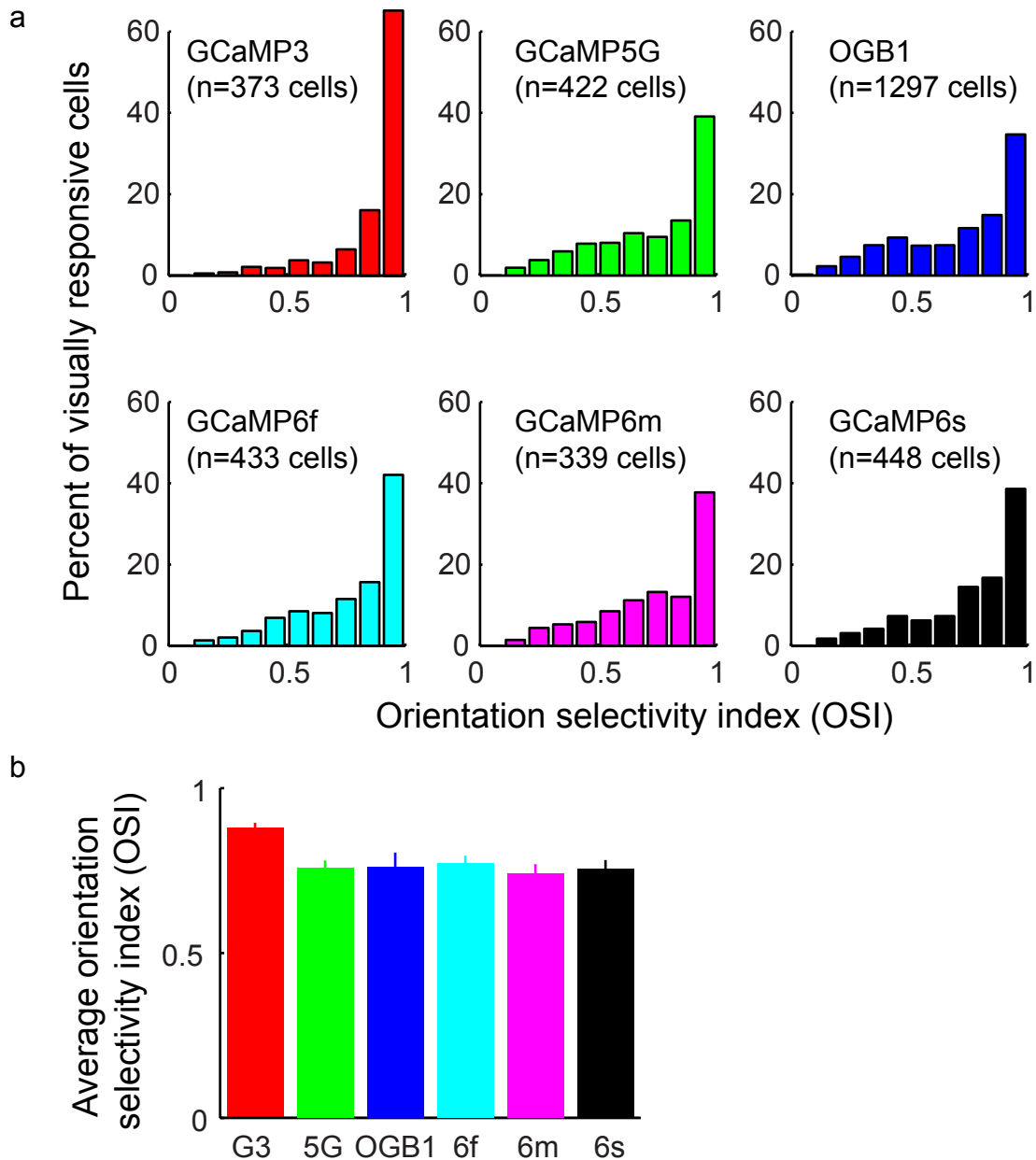
c, Examples of neurons with filled and excluded nuclei at various times after infection. Left, nuclear filled cells can display tuned responses within ~1-2 month after virus injection, albeit with a longer fluorescence decay time. Middle, 158 days post infection, tuned responses are routinely observed in nucleus excluded cells. Right, 158 days post infection, tuned responses are rarely seen in nuclear filled cells.

d, Percentage of orientation selective cells remained relatively constant over time for nucleus excluded cells (black) but decreased over time for nucleus filled cells (red).



Supplementary Figure 8 | Reproducible GCaMP6s V1 responses across trials.

The response amplitude was averaged over 448 cells and plotted against trial number. No stimulus adaptation was evident.

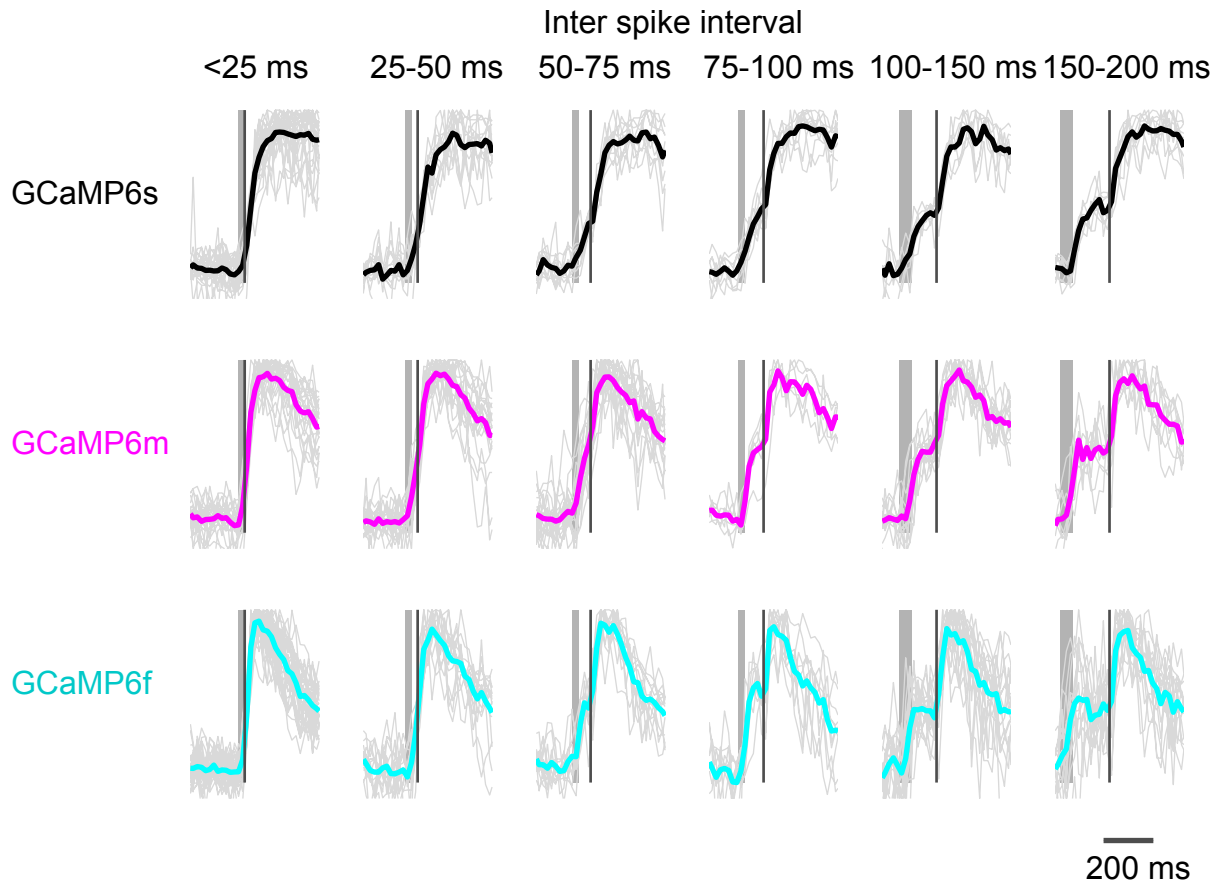


Supplementary Figure 9 | Comparison of orientation tuning in V1 neurons measured with different sensors.

a, Distribution of orientation selectivity index (OSI) for visually responsive cells measured using different sensors.

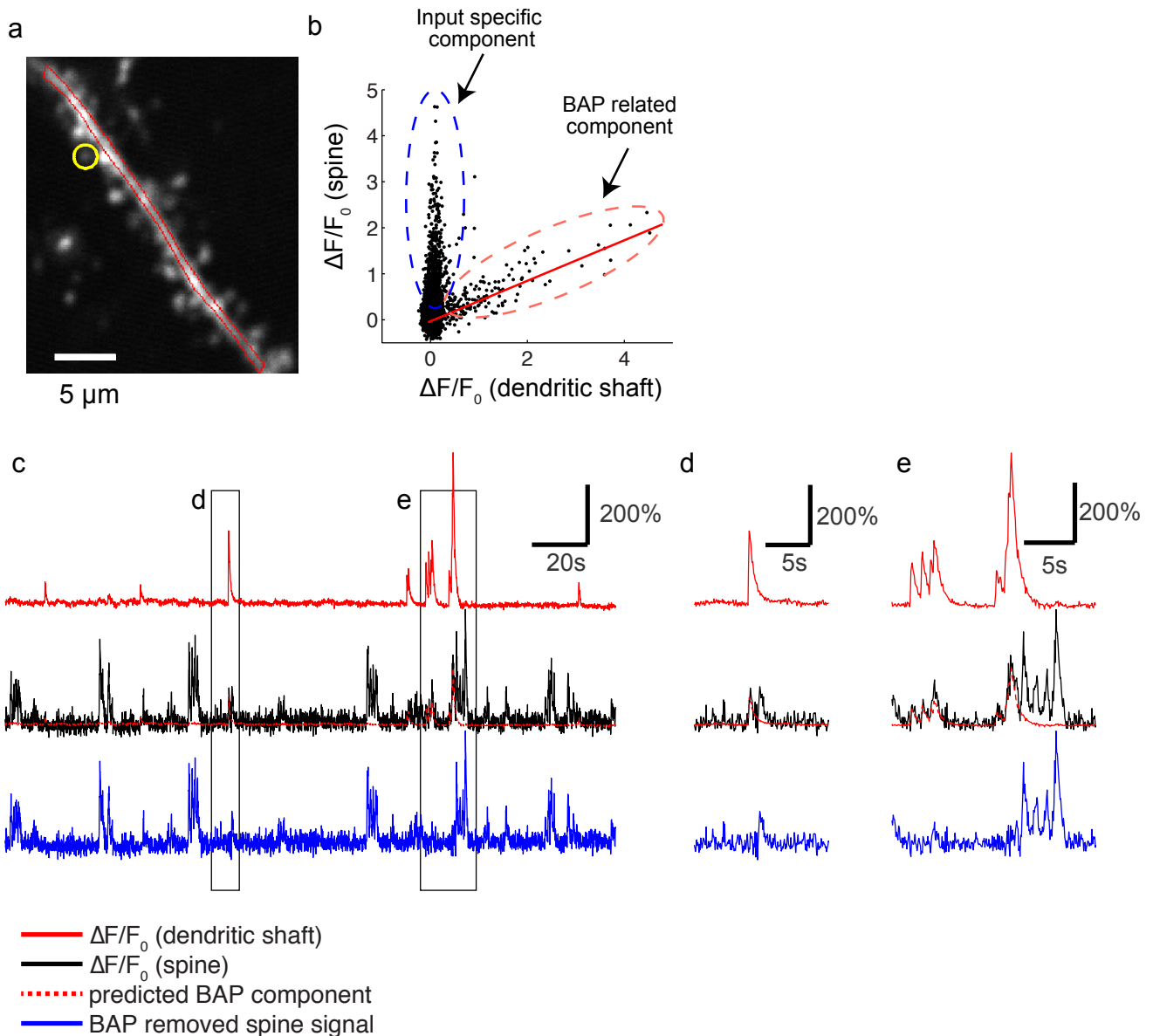
b, Average OSI across sensors (mean ± s.e.m.).

Peak normalized 2AP response aligned to the second spike



Supplementary Figure 10 | Temporal resolution of different GCaMP6 sensors in the visual cortex.

Average fluorescent response to 2 action potentials sorted by the inter spike intervals (ISI) and aligned to the second spike (gray line). Shaded areas indicate the window where the first spike occurred. The second spike can be resolved temporally as stepwise increases in fluorescent response for a minimal ISI of 50-75ms (GCaMP6f), 75-100ms (GCaMP6m) and 100-150 ms (GCaMP6s).



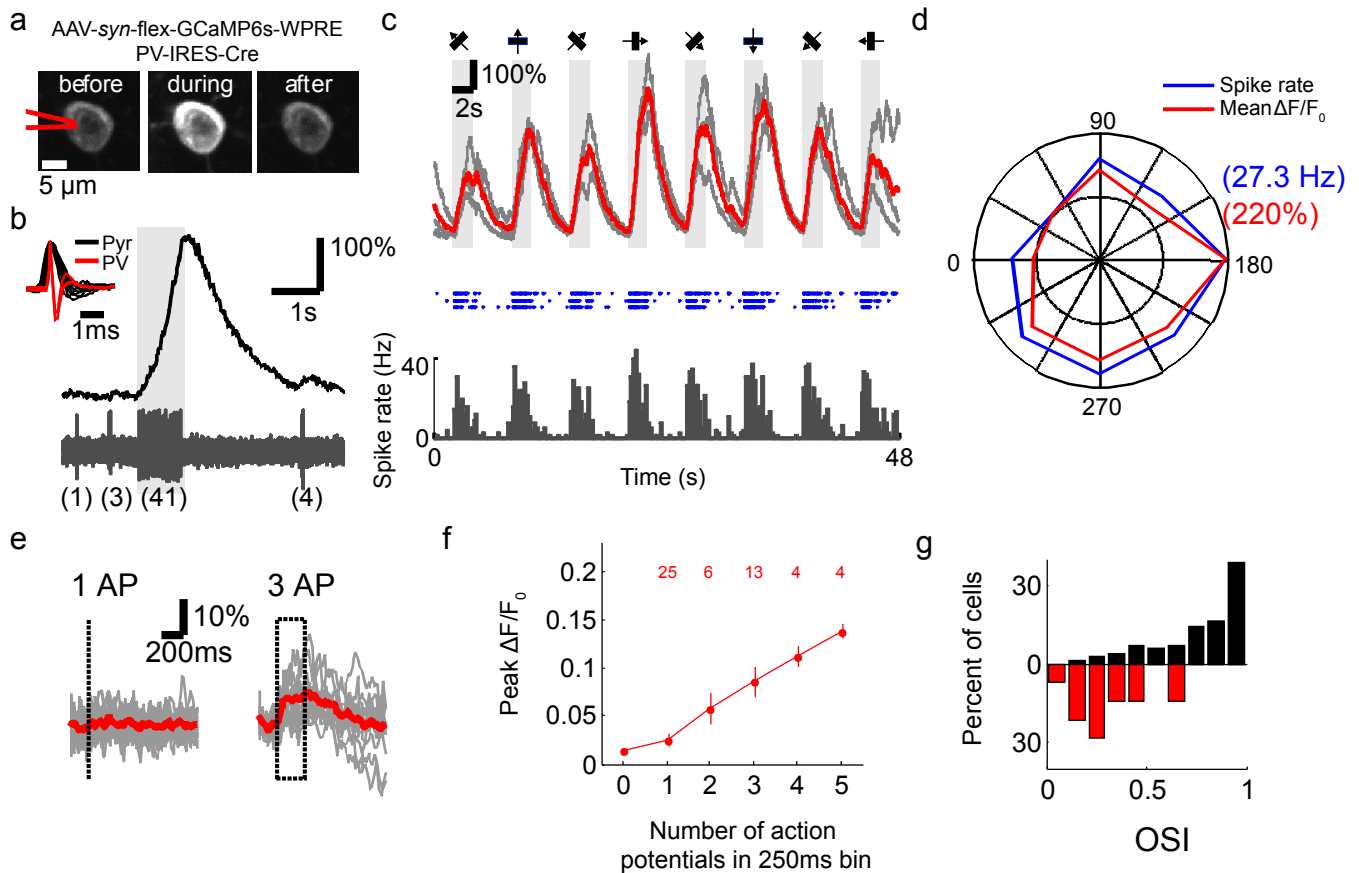
Supplementary Figure 11 | Isolating input specific spine signal.

a, A segment of pyramidal cell dendrite labeled with GCaMP6s. A region covering the parent dendritic shaft (red) was drawn to measure global, BAP related dendritic signal. Spine signals were measured from circular regions covering individual spines (yellow).

b, Contribution of the global dendritic signal to the spine signal was estimated using robust regression.

c, Example dendritic shaft signal (red), spine signal (black), the predicted BAP component of the spine signal (dash red line; *i.e.*, shaft signal scaled by the slope of the fitted line in **b**), and BAP removed, input specific spine signal (blue).

d,e, Enlarged view of the boxed regions in **c**.



Supplementary Figure 12 | GCaMP6s signals in PV-positive interneurons in the visual cortex and their relationship to action potentials.

a, Image of a PV neuron labeled with GCaMP6s before (left), during (middle) and after (right) visual stimulation (as in Figure 2).

b, Fluorescence signal (top) and simultaneously recorded spikes (bottom) of a PV cell in response to visual stimulation. The number of spikes in each burst is indicated below the spike trace. Inset, averaged spike waveform of recorded PV cells (red) compared to pyramidal cells (black, recorded in wild-type mice).

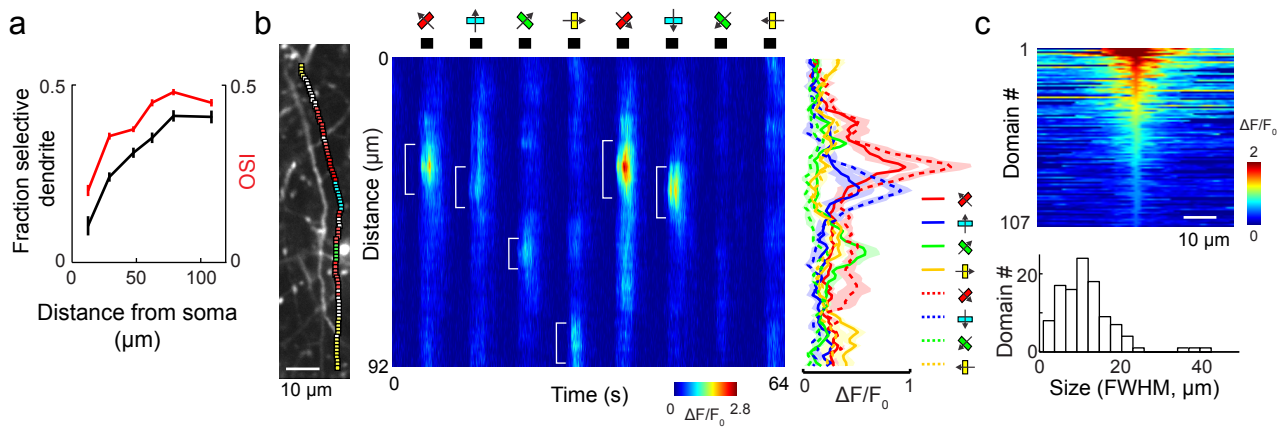
c, Fluorescence response of a GCaMP6s labeled PV cell (top, gray: individual trial; red, average of 3 trials) and corresponding spike raster (middle) and peristimulus time histogram (bottom) during the presentation of eight drifting grating stimuli.

d, Mean fluorescence response (red) and spike rate (blue) of the neuron in (c) in response to gratings with different orientations.

e, Fluorescence change in response to one (left) and three (right) APs. Gray: single trials; Red: average of all trials.

f, Fluorescence change as a function of number of action potentials in a 250 ms bin.

g, Distribution of orientation selectivity index (OSI) of PV cells (red) and pyramidal cells (black).

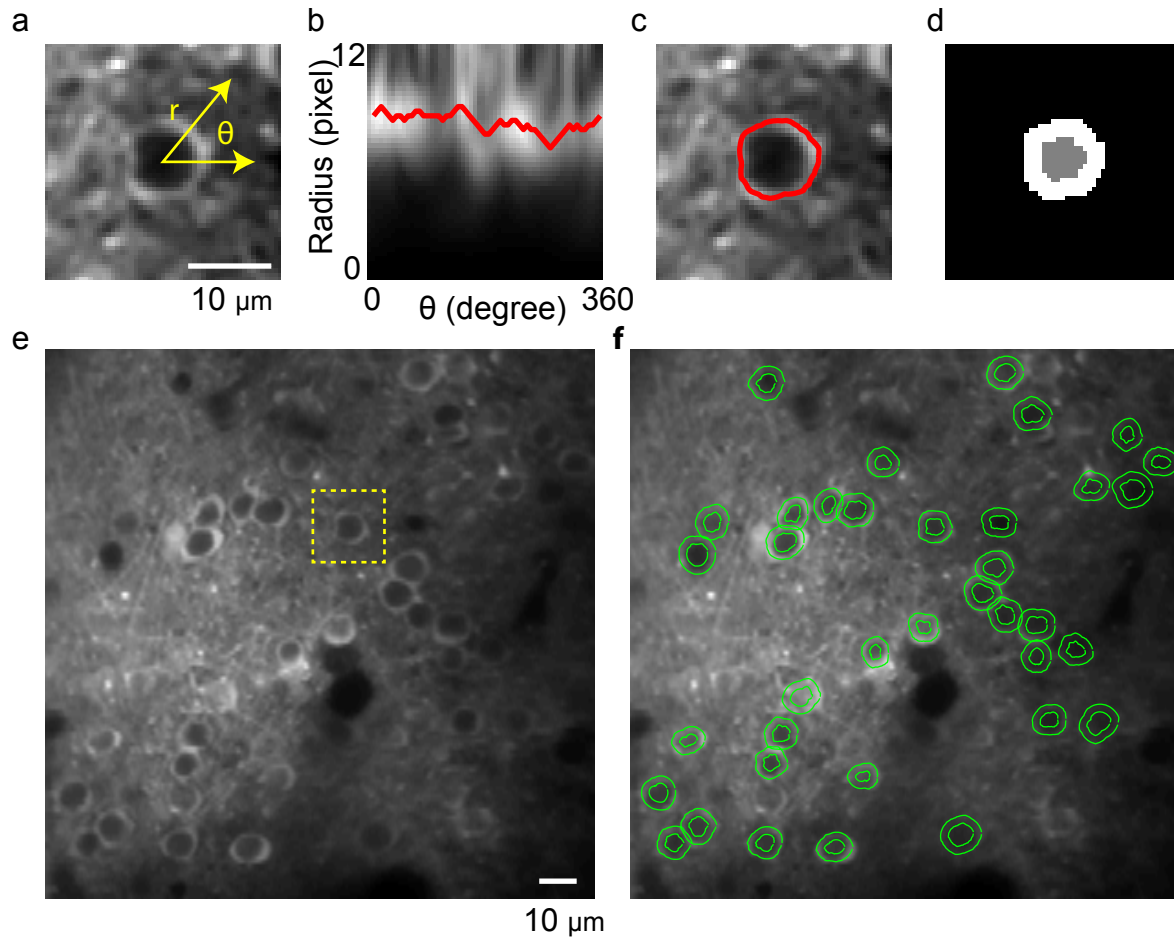


Supplementary Figure 13 | Properties of visual cortical interneuron dendrites.

a, OSI and fraction of orientation-selective dendritic sites plotted against the distance from soma (3425 sites, 5 cells).

b, Left, a dendritic segment labeled with GCaMP6s. Orientation-selective sites are indicated by colored squares. Middle, color-coded fluorescence responses of 92 dendritic ROIs (1 micrometer spacing) averaged over 5 trials. Each row shows the response of one ROI. White brackets indicate dendritic domains with peak $\Delta F/F_0 > 40\%$. Right, spatial distribution of peak $\Delta F/F_0$ averaged over two second stimulus periods. Colors correspond to stimulus orientations.

c, Top, spatial profiles for 107 dendritic domains (peak $\Delta F/F_0 > 40\%$) aligned to the location of the peak response. Bottom, distribution of the domain sizes.



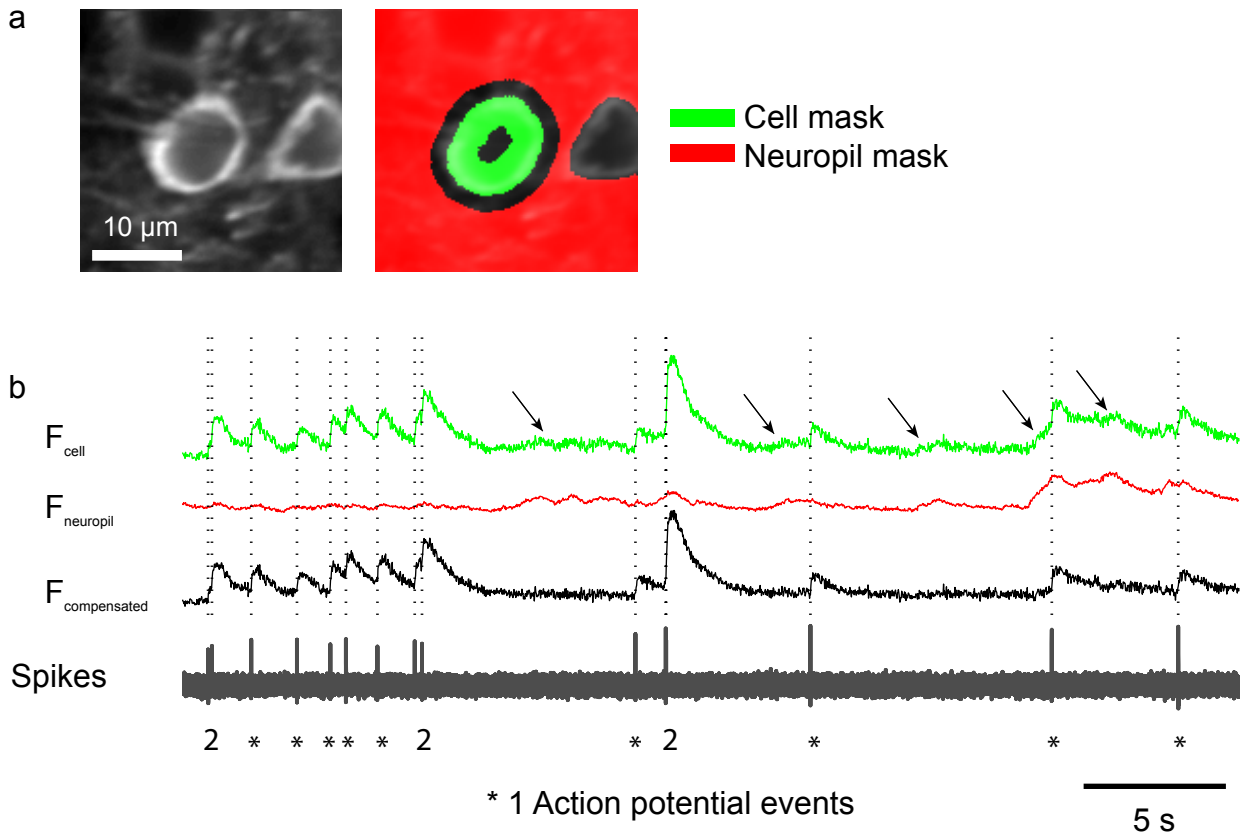
Supplementary Figure 14 | Algorithm to define regions of interest.

a, A typical GCaMP-labeled cell, showing the ring-shaped cytoplasm. The algorithm starts with manual selection of the cell center. The intensity profile is then computed in polar coordinates around the cell center **b**, and a closed path (red curves in **b** and **c**) is determined that maximizes the summed intensity along the path.

d, An example region of interest output by the algorithm.

e, An example field of view with multiple GCaMP-labeled cells.

f, Regions of interest covering GCaMP labeled cells in the field of view.



Supplementary Figure 15 | Neuropil subtraction is required to compute signals determined by somatic spikes.

a, Left, a GCaMP6s labeled cell targeted for cell attached recording. Right, regions where somatic (green) and neuropil (red) fluorescence were measured.

b, From top to bottom: averaged fluorescence of the cell region, average fluorescence of surrounding neuropil region, estimated true fluorescence of the cell after neuropil compensation, and simultaneously recorded spikes. Fluorescence changes not related to spikes (arrows) were removed after neuropil subtraction.

Supplementary Table 1 | GCaMP sensor comparison in dissociated neuronal culture.

Sensor	Baseline fluorescence F_0 , relative to GCaMP3	Dynamic range ($\Delta F/F_0$ at 160 AP)	Decay $\tau_{1/2}$ 10 AP (ms)	Rise τ_{peak} 10 AP (ms)	SNR 1 AP (fold GCaMP3)	SNR 10 AP (fold GCaMP3)
GCaMP3	100±3%	565±6%	597±8	137±4	1.0±0.1	1.0±0.03
GCaMP5G	72±3%	1085±66%	667±43	166±20	1.7±0.3	1.4±0.2
GCaMP6s	74±5%	1680±48%	1796±73	480±24	11.2±2	4.6±0.8
GCaMP6m	54±4%	1177±30%	1162±55	280±48	10.3±1.7	3.1±0.3
GCaMP6f	67±5%	1314±56%	400±41	80±35	6.2±2	4.1±0.3

Supplementary Table 2 | Biophysical properties of purified GCaMP sensors.

Selected GCaMP variants were cloned into a pRSET bacterial expression construct and transformed into *E. coli* for analysis as purified proteins¹⁶. T7 Express bacteria (NEB) were grown in 100 mL of ZYM-5052 autoinduction media⁷⁰ containing 100 µg/mL ampicillin at 30°C for 48 h. Bacterial pellets were resuspended in 10 mL of B-PER (ThermoScientific) and lysed with 1 mg/mL lysozyme and 15 U/mL DNase, and lysates were cleared by centrifugation. Supernatants were applied to 500 µL of Ni²⁺-charged Profinity IMAC resin (Bio-Rad) in gravity columns. The resin was washed with 80 column volumes of 20 mM Tris, pH 8.0, 300 mM NaCl, 1 mM imidazole followed by 20 column volumes of 20 mM Tris, pH 8.0, 500 mM NaCl, 10 mM imidazole, and GCaMP variants were eluted in 750 µL of 20 mM Tris, pH 8, 100 mM NaCl, 100 mM imidazole.

Calcium titrations were done using EGTA-buffered Ca²⁺ solutions (Calcium Calibration Buffer Kit #1, Life Technologies). Purified GCaMP variants were diluted 1:50 in quadruplicate in 30 mM MOPS, pH 7.2, 100 mM KCl containing either 10 mM EGTA (zero free calcium) or 10 mM CaEGTA (~39 µM free calcium). These two stocks were mixed in various ratios to give 11 different free calcium concentrations. Green GCaMP fluorescence (excitation 485 nm, 5 nm bandpass; emission 510 nm, 5 nm bandpass) was measured using a Safire2 plate reader (Tecan). Dynamic range was determined from the 0 and 39 µM free Ca²⁺ points. Sigmoidal binding functions were fit to the calcium titration fluorescence data to extract the Hill coefficient and K_d for Ca²⁺ for each GCaMP variant. k_{off} was determined from a single exponential fit to the fluorescence decay following rapid mixing of the protein samples in 1 µM calcium with a solution of 10 mM BAPTA at room temperature, both buffered with 50 mM MOPS, 100 mM KCl at pH 7.2, using a stopped-flow device (Applied Photophysics) coupled to a fluorometer (Varian). pH titrations were carried out by diluting concentrated purified proteins into pH buffers containing 50 mM citrate, 50 mM Tris, 50 mM glycine, 100 mM NaCl, and either 5 mM CaCl₂ or 5 mM EGTA that were pre-adjusted to twelve different pH values between 4.5 and 10.5. pK_a values were determined from the inflection point of a sigmoid fit to fluorescence versus pH. To determine chromophore extinction coefficients (ε_{apo} and ε_{sat}), absorbance of purified GCaMP variants in 50 mM MOPS, 100 mM KCl, pH 7.2 with either 5 mM CaCl₂ or 10 mM EGTA was measured at 497 nm or 505 nm, respectively. Chromophore concentration was then quantitated by denaturing the protein sample in 0.1 M NaOH and using the extinction coefficient 44,000 M⁻¹cm⁻¹ at 447 nm for denatured GFP chromophore. Quantum yields (Φ_{sat}) of calcium-saturated GCaMP variants in 50mM MOPS, 100mM KCl, 5mM CaCl₂ were measured directly with an integrating-sphere spectrometer (Quantaaurus-QY, Hamamatsu). Values are mean ± standard deviation for three independently purified protein samples. All variants have the same calcium-free and calcium-bound excitation/emission peaks of 505 nm/517 nm and 497 nm/515 nm, respectively. Size exclusion chromatography was also performed with 20 µM protein, and the GCaMP3, GCaMP5G, and GCaMP6 variants all were >95% monomeric with or without calcium.

Sensor	Dynamic range (F _{max} /F _{min})	K _d (nM)	Hill coefficient	k _{off} (s ⁻¹)	pK _{a, apo}	pK _{a, sat}	ε _{apo} (x1000) (M ⁻¹ cm ⁻¹)	ε _{sat} (x1000)	Φ _{sat}
GCaMP3	13.5±0.7	345±17	2.54±0.04	2.57	8.44±0.01	7.13±0.07	4.6±0.1	32.6±1.5	0.62±0.02
GCaMP5G	45.4±0.9	447±10	2.46±0.04	2.52	8.61±0.15	6.58±0.02	2.6±0.1	54.3±0.3	0.59±0.01
GCaMP6s	63.2±3.1	144±4	2.90±0.17	1.12	9.77±0.70	6.20±0.02	2.91±0.04	68.5±0.1	0.610±0.004
GCaMP6m	38.1±1.8	167±3	2.96±0.04	2.06	8.68±0.09	6.90±0.04	2.07±0.04	38.2±0.9	0.61±0.01
GCaMP6f	51.8±2.8	375±14	2.27±0.10	3.93	8.77±0.16	6.34±0.01	2.80±0.03	61.9±0.4	0.590±0.002

Supplementary Table 3 | GCaMP comparison in mouse V1 *in vivo* (cell attached recording).

Sensor	$\Delta F/F_0$, 1 AP	Decay $\tau_{1/2}$ 1 AP (ms)	Rise τ_{peak} 1AP (ms)	Detection efficiency (at 1 % false positive)
GCaMP5K	3.6±1.9 %	268±20	60±20	19±12%
GCaMP6s	23±3.2 %	550±52	179±23	99±0.2%
GCaMP6m	13±0.9 %	270±23	80±7	94±0.5%
GCaMP6f	19±2.8 %	142±11	45±4	84±6%

Supplementary Table 4 | GCaMP comparison in *Drosophila* larval NMJ.

Sensor	$\Delta F/F_0$, 1 Hz	$\Delta F/F_0$, 20 Hz	Decay time, $\tau_{1/2}$ 20 Hz (s)	Rise time to peak after stimulus offset, 20 Hz (s)
GCaMP5G	0.0210±0.0020	1.3123±0.0787	0.6075±0.0131	0.1546±0.0074
GCaMP6s	0.0454±0.0029	4.8598±0.2040	1.1448±0.0223	0.1626±0.0027
GCaMP6m	0.0751±0.0058	5.5028±0.3032	0.8718±0.0372	0.1427±0.0117
GCaMP6f	0.0337±0.0024	2.3000±0.2438	0.3796±0.0094	0.1415±0.0059

- 65 Lister, J. A., Robertson, C. P., Lepage, T., Johnson, S. L. & Raible, D. W. nacre encodes a zebrafish microphthalmia-related protein that regulates neural-crest-derived pigment cell fate. *Development* **126**, 3757-3767 (1999).
- 66 White, R. M. *et al.* Transparent adult zebrafish as a tool for in vivo transplantation analysis. *Cell Stem Cell* **2**, 183-189, (2008).
- 67 Westerfield, M. *The zebrafish book : a guide for the laboratory use of zebrafish (Brachydanio rerio)*. (M. Westerfield, 1993).
- 68 Asakawa, K. *et al.* Genetic dissection of neural circuits by Tol2 transposon-mediated Gal4 gene and enhancer trapping in zebrafish. *Proc. Natl Acad. Sci. USA* **105**, 1255-1260, (2008).
- 69 Akitake, C. M., Macurak, M., Halpern, M. E. & Goll, M. G. Transgenerational analysis of transcriptional silencing in zebrafish. *Dev. Biol.* **352**, 191-201, (2011).
- 70 Studier, F. W. Protein production by auto-induction in high density shaking cultures. *Protein Expr. Purif.* **41**, 207-234 (2005).